ARTICLE

Area-Selective Atomic Layer Deposition Patterned by Electrohydrodynamic Jet Printing for Additive Manufacturing of Functional Materials and Devices

Tae H. Cho, Nazanin Farjam, Christopher R. Allemang, Christopher P. Pannier, Eric Kazyak, Carli Huber, Mattison Rose, Orlando Trejo, Rebecca L. Peterson,* Kira Barton,* and Neil P. Dasgupta*

Read Online

ACCESS | Metrics & More | Article Recommendations | SI Supporting Information

ABSTRACT: There is an increasing interest in additive nanomanufacturing processes, which enable customizable patterning of functional materials and devices on a wide range of substrates. However, there are relatively few techniques with the ability to directly 3D print patterns of functional materials with sub-micron resolution. In this study, we demonstrate the use of additive electrohydrodynamic jet (e-jet) printing with an average line width of 312 nm, which acts as an inhibitor for area-selective atomic layer deposition (AS-ALD) of a range of metal oxides. We also demonstrate subtractive e-jet printing with solvent inks that dissolve polymer inhibitor layers in specific regions, which enables localized AS-ALD within those regions. The chemical selectivity and morphology of e-jet patterned polymers towards binary and ternary oxides of ZnO, Al_2O_3, and SnO_2 were quantified using X-ray photoelectron spectroscopy, atomic force microscopy, and Auger electron spectroscopy. This approach enables patterning of functional oxide semiconductors, insulators, and transparent conducting oxides with tunable composition, Å-scale control of thickness, and sub-μm resolution in the $x−y$ plane. Using a combination of additive and subtractive e-jet printing with AS-ALD, a thin-film transistor was fabricated using zinc−tin-oxide for the semiconductor channel and aluminum-doped zinc oxide as the source and drain electrical contacts. In the future, this technique can be used to print integrated electronics with sub-micron resolution on a variety of substrates.

KEYWORDS: additive manufacturing, atomic layer deposition, electrohydrodynamic jet printing, area-selective deposition, printable electronics
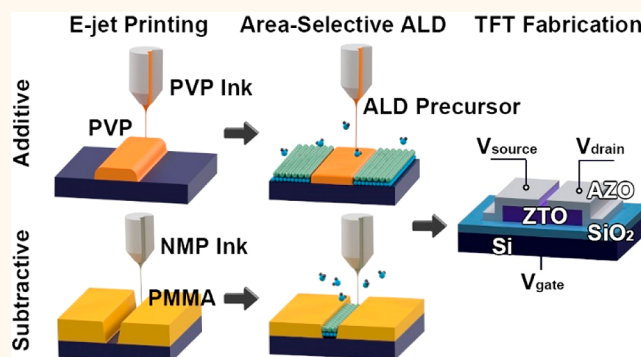
There is an increasing demand for customization in the manufacturing of integrated nanosystems, which has motivated the development of customizable, printable devices for specific end-user requirements.[1,2] The current state-of-the-art in nanofabrication of functional devices involves multiple lithographic patterning steps, combined with thin-film deposition and top-down etching processes. Advances in nanofabrication processes have led to the high-volume fabrication of 5 nm node technology with ultra-low defect density and tight process control.[3] While lithographic processes have advantages in resolution and process reliability, they are not ideal for rapid customization and require complex tooling inside a costly and resource-intensive cleanroom environment. In contrast, additive manufacturing processes enable rapid prototyping of 3D structures that can be tuned on-the-fly, and can be integrated in a bottom-up manner on top of non-planar, flexible substrates.[2]
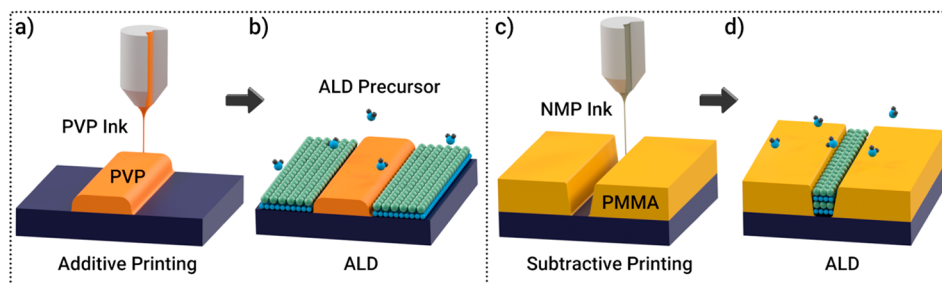
Despite the benefits of additive nanomanufacturing, trade-offs exist among spatial resolution, throughput, cost, and compatibility with a broad range of materials. Current nanoscale printing techniques can only process a limited
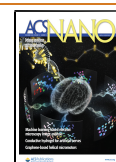
Scheme 1. Process Flow for AS-ALD Using e-Jet Printing[a]

[a](a and b) Additive e-jet printing of a polymer inhibition layer locally inhibits ALD growth in the printed region. (c and d) Subtractive printing uses a solvent ink to dissolve and displace an inhibition layer, generating an exposed region where ALD growth locally occurs.

range of functional materials, due to strict requirements in the physical/chemical properties of the ink, which influence the chemical, structural, and morphological properties of the resulting printed materials.[1,2] Furthermore, existing techniques often require long processing times. Scanning-probe-microscopy (SPM)-based techniques, such as dip-pen nanolithography and scanning tunneling microscopy (STM) lithography, are capable of generating complex 3D structures with <10 nm resolution.[2,3,5] However, SPM-based techniques are often limited by a high system cost and low line speed (1−10 nm/s for STM and AFM manipulation), which requires long time periods to print over large areas.[1] Alternatively, direct laser writing (DLW) using two-photon polymerization (2PP) enables 3D patterning of polymers with ∼100 nm resolution and line speeds up to 100 μm/s.[1,6,7] However, these systems rely on expensive femtosecond laser equipment and are restricted to a subset of photoactive polymers.

In contrast, direct printing techniques, such as inkjet printing, have lower system costs and are compatible with a wide range of ink materials. Inkjet printing can also achieve orders of magnitude higher line speeds than SPM or DLW techniques (> 50 mm/s), which enables faster printing over large areas.[1,8,9] However, unless complicated self-alignment schemes are used,[10−13] conventional inkjet printing can achieve down to 20 μm resolution in the substrate plane and can only print low viscosity materials (5−20 mPa s) due to the pressure required to extrude the ink out of the nozzle.[8,9] Therefore, an overall challenge of the additive nanomanufacturing is that there is no universal technique that simultaneously achieves high resolution, low cost, and high patterning speed of a wide range of materials.

To overcome these trade-offs, electrohydrodynamic jet (e-jet) printing has emerged as an alternative to inkjet printing, which maintains a low system cost and is compatible with a wide range of materials and high line speeds (>50 mm/s), while enabling sub-micrometer resolution.[13] E-jet is an additive printing technique that uses an applied electric field to pull ink out of a conductive nozzle. Compared to inkjet printing, the ink flow can be controlled more precisely in e-jet by using smaller-diameter nozzles (sub-micron), and can also overcome higher pressure requirements to eject the ink by taking advantage of electrohydrodynamic phenomena. E-jet allows for fast and versatile printing with higher resolution (down to ∼30 nm features) and a broad range of ink viscosities (1−500 000 mPa s).[14,15] Previous studies have demonstrated that functional devices can be fabricated with e-jet printed layers.[16−18] However, the range of functional materials that can be e-jet printed are typically limited by available ink compositions. This

motivates the need to combine e-jet printing with complementary deposition processes that enable tuning of material composition, structure, and thickness at the atomic scale.

Atomic layer deposition (ALD) is a surface reaction-controlled, vapor-phase thin-film deposition technique that allows for conformal coating of high aspect ratio structures.[19,20] ALD is widely used in the semiconductor industry, as it allows for tuning of material composition and thickness with sub-nanometer precision.[19,21] However, most ALD growth conditions result in blanket coverage of a substrate surface, which requires an additional patterning step to control growth in the substrate plane.[22−24]

To overcome the limitations of traditional lithographic patterning and alignment, there has been significant progress in the development of area-selective ALD (AS-ALD) processes, which intrinsically control the location of ALD growth as-deposited.[22,24] In AS-ALD, the substrate surface is partially covered with an inhibition layer (typically either a self-assembled monolayer or polymer) that lacks the required surface functional groups for ALD nucleation and growth. Various inhibitor materials have been reported to prevent the growth of ALD oxides, nitrides, and metallic films.[25−31] Therefore, by patterning an inhibition layer in 3-D, additive manufacturing of functional materials and devices can be achieved with atomically precise control.

AS-ALD patterns have been previously formed using a range of techniques including direct printing, electron-beam induced deposition (EBID), and/or directed self-assembly of templates.[22,24,26,32−34] For example, seed layers patterned by EBID and μ-plasma printing have been used to locally deposit ALD films by activating the surface.[26,34,35] Inkjet printing has been demonstrated to define an AS-ALD pattern; however, the resolution limit of inkjet-printed polymers produced device dimensions greater than 50 μm.[28,36,37] Additionally, patterning of SAMs using micro-contact printing or selective growth on pre-patterned surfaces has been widely explored.[25,33,38,39] However, uniform SAMs with fully packed, low defect densities typically require a long formation time (on the order of hours) and are limited to deposition on specific surface functional groups.[22,25,40] In contrast, organic polymers such as poly(methyl methacrylate) (PMMA) and polyvinyl-pyrrolidone (PVP) can be quickly and easily spin-coated or printed, which motivates their use as inhibitors in this work.

The goal of this study is to combine e-jet printing of polymers with AS-ALD to realize an additive manufacturing platform with sub-μm spatial resolution in the x- and y-directions and sub-nm resolution in the z-direction. In addition, ALD enables atomically precise control of material
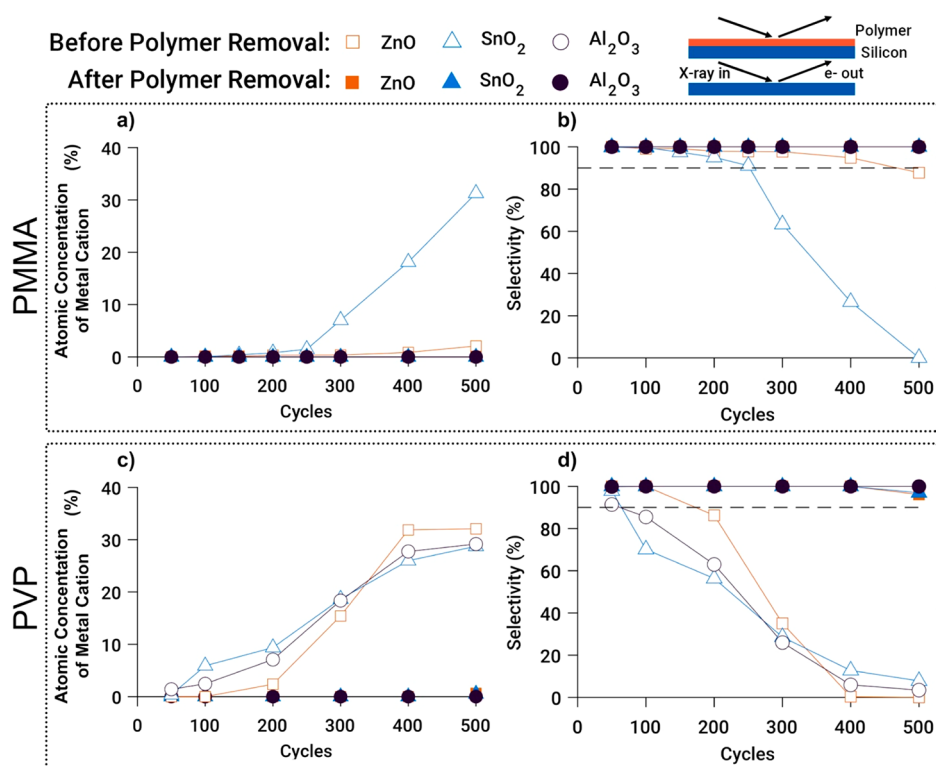
Figure 1. Atomic composition and selectivity of the metal cation in the binary ZnO, Al$_2$O$_3$, and SnO$_2$ grown by ALD at 130 °C on (a and b) PMMA and (c and d) PVP surfaces, obtained by XPS. ZnO was deposited using diethylzinc (DEZ), Al$_2$O$_3$ was deposited using dimethylaluminum isopropoxide (DMAI), and SnO$_2$ was deposited using tetrakis (diethylamino) tin(IV) (TDMASn).

composition, which we can exploit to tune the electronic properties of ternary oxide semiconductors including zinc−tin-oxide (ZTO) and aluminum-doped zinc oxide (AZO).

We demonstrate two approaches to e-jet printing of AS-ALD patterns: (1) additive printing of inhibitor patterns using a polymer ink; and (2) subtractive printing of pre-deposited polymer inhibitor layers using a solvent ink as shown in Scheme 1. The chemical selectivity of the patterned films was quantified using Auger electron spectroscopy (AES) and X-ray photoelectron spectroscopy (XPS), while nanoscale morphology was analyzed using atomic force microscopy (AFM) and scanning transmission electron microscopy (STEM). Using this approach, bottom-gate, top-contact ZTO thin-film transistors (TFTs) were fabricated. TFTs made using this method are well-behaved, with an on/off current ratio of greater than 10^5. In the future, the combination of e-jet with AS-ALD could enable additive nanomanufacturing of electronic devices on a variety of substrates, such as flexible or non-planar substrates, without the need for traditional lithography.

RESULTS

In AS-ALD processes, the patterned inhibitor layer needs to be chemically inert towards the ALD precursors in order to selectively inhibit growth. When the surface is terminated with thermodynamically unfavorable functional groups, no ligand exchange occurs with the ALD precursor.[24,42] Previous work used the log of the acid dissociation constant, pK_a, of different polymers to measure the relative extent of dissociation (proton liability), which was also shown to influence inhibition behavior.[36] In addition, the reaction rate may be kinetically limited if there is a large activation barrier for the ligand exchange reactions between the ALD precursors and the

surface functional groups.[25,43,44] In practice, there often exists a threshold number of cycles, beyond which ALD growth initiates on top of the inhibitor layer; this threshold determines the selectivity window.[22,45] In this study, PMMA and PVP were chosen as inhibition layers, owing to their high selectivity against growth of several ALD materials.[28,46−48]

To demonstrate the inhibition behavior of the binary and ternary oxides in this study, PMMA and PVP films were first spin-coated on Si. These substrates were then exposed to varying numbers of ALD cycles of ZnO, Al$_2$O$_3$, and SnO$_2$, and the surface composition was analyzed by XPS, with the results shown in Figure 1.

To quantify the selectivity window of the inhibitor polymers to ALD growth, the selectivity, S_x, was defined as shown in eq 1:

$$S_x = \frac{R_{gs} - R_{ns}}{R_{gs} + R_{ns}}$$

(1)

where R_{gs} represents the atomic percentage of the metal cation on the growth surface (a bare silicon wafer), and R_{ns} represents that of the nongrowth surface (PMMA and PVP films).[24,45] The selectivity window was defined as the ALD cycle number when the selectivity drops below 90%.

As shown in Figure 1a, no ALD growth was observed on the PMMA surface during the initial 100 cycles. On PVP, no ZnO growth was observed in the initial 100 cycles, and the atomic percentage of Al and Sn was less than 2% after the first 50 cycles (Figure 1c). The observed differences in selectivity between the inhibitors can be partially attributed to the surface functional groups present in the polymers.[32,42,43]

The selectivity of PMMA, as defined by eq 1, drops below 90% at 500 cycles (92.4 nm) for ZnO and 300 cycles (25.6
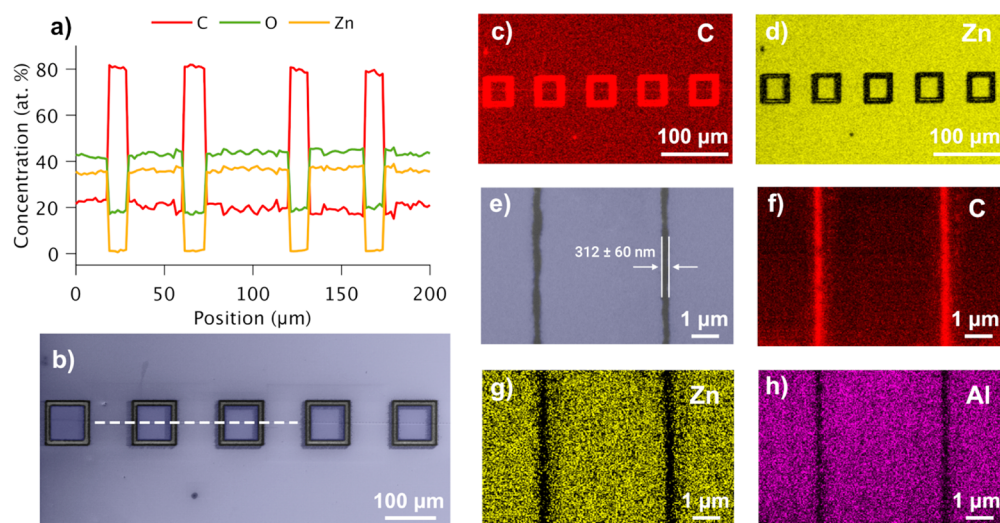
Figure 2. Additive printing of PVP for AS-ALD: (a) AES line scan of the additive e-jet printed PVP pattern after 100 cycles of ZnO-ALD (19 nm). (b) SEM image of the PVP patterned sample. AES elemental maps are provided for key elements: (c) carbon map and (d) zinc map. (e) SEM image of additively printed 312 ± 60 nm wide PVP pattern after 10 supercycles of AZO ALD (20 nm). (f−h) Corresponding AES elemental map scans carbon, zinc, and aluminum, respectively.

nm) for SnO$_2$, while Al$_2$O$_3$ growth is suppressed even after 500 cycles (58.2 nm), as shown in Figure 1b. For PVP surfaces, the selectivity window is not as well-defined for ZnO, SnO$_2$, and Al$_2$O$_3$ in the as-deposited samples.

As the inhibitor is sequentially exposed to a higher number of ALD cycles, the precursors eventually react at selective nucleation points on the surface. This leads to the formation of small islands on the polymer surface, which can coalesce into a continuous film as growth proceeds.[24] Depending on the precursor molecule and the inhibition polymer, the selectivity window may differ quite significantly.[22,49] For instance, it has been shown that ALD of Al$_2$O$_3$ using trimethylaluminum (TMA) starts to nucleate on a PMMA surface during the initial 10 cycles, whereas the surface remains selective up to 850 Å if dimethylaluminum isopropoxide (DMAI) is used as the precursor.[22,28] For this reason, we chose DMAI as the Al precursor in this study.

We note that ALD within the bulk of non-reactive polymers is also possible when sub-surface diffusion occurs, due to physical entrapment of gas molecules.[50,51] This modification of the bulk polymer can potentially affect its solubility. Additionally, precursor diffusion through the polymer thickness may result in film growth on the substrate surface below the polymer, which would remain even after polymer removal.[30] When cross-sectional scanning transmission electron microscopy with energy dispersive spectroscopy (STEM-EDS) was performed on PMMA and PVP layers after exposure to 300 cycles of SnO$_2$, PMMA exhibited an abrupt interface while PVP exhibited a vapor phase infiltration regime, suggesting that sub-surface infiltration occurs more readily on the PVP (Figure S3).[51] These results are consistent with the improved selectivity of PMMA compared to PVP for SnO$_2$, shown in Figure 1.

Defective growth on the inhibitor surface beyond the selectivity window is the main challenge to achieve highly selective AS-ALD. However, an additional advantage of printing organic polymers such as PMMA and PVP is that island growth beyond the selectivity window facilitates easy removal of the polymer (and any ALD islands) by dissolution in solvents, since the majority of the polymer surface is still exposed. Therefore, to verify complete removal of the polymer without any deposition at the Si−polymer interface, PMMA and PVP-coated silicon substrates were soaked in acetone and methanol, respectively, for 30 min after ALD processing, and were analyzed using XPS.

As shown in Figure 1c and 1d, metal cation peaks from the ALD precursors (Zn, Sn, and Al) were absent in the XPS spectra after polymer removal, demonstrating complete removal of the polymer without any ALD growth on the underlying Si surface. This shows that the defective deposition on top of the inhibitor can be removed in order to maintain high selectivity on the non-growth surface. Furthermore, when the thickness of PVP was increased from 60 to 120 nm, the selectivity after polymer removal increased to a higher number of cycles, which is attributed to a longer path length for bulk diffusion through the polymer (Figure S2).

Beyond binary oxides, ALD is a powerful technique to fabricate complex multi-element films with precise control of stoichiometry.[52−57] This enables deposition of functional materials with tunable electrical properties. Therefore, the inhibition behaviors of ternary and doped oxides were investigated using ZTO and AZO. ZTO was chosen as a semiconductor layer owing to its use in TFTs that do not require scarce elements such as In and Ga.[21,58,59] Amorphous ZTO semiconductor films have been shown to exhibit high electron mobility, and ALD can be used to tune the zinc to tin ratio and the thickness of the film precisely.[54,60−62] AZO was chosen as a representative conductive oxide since it exhibits low electrical resistivity.[63,64] Consistent with the binary oxide selectivity data, AZO and ZTO films deposited with the conditions used in this study (see Methods Section) demonstrated inhibition behavior on PMMA and PVP during the initial ALD cycles, as confirmed by XPS analysis (Figure S1).

To demonstrate the potential of e-jet printing for patterning AS-ALD for device fabrication, additive printing of PVP inhibitors (as shown in Scheme 1) was first explored. Elemental compositions of as-deposited ZnO, AZO, and ZTO films on e-jet printed patterns were analyzed using AES.
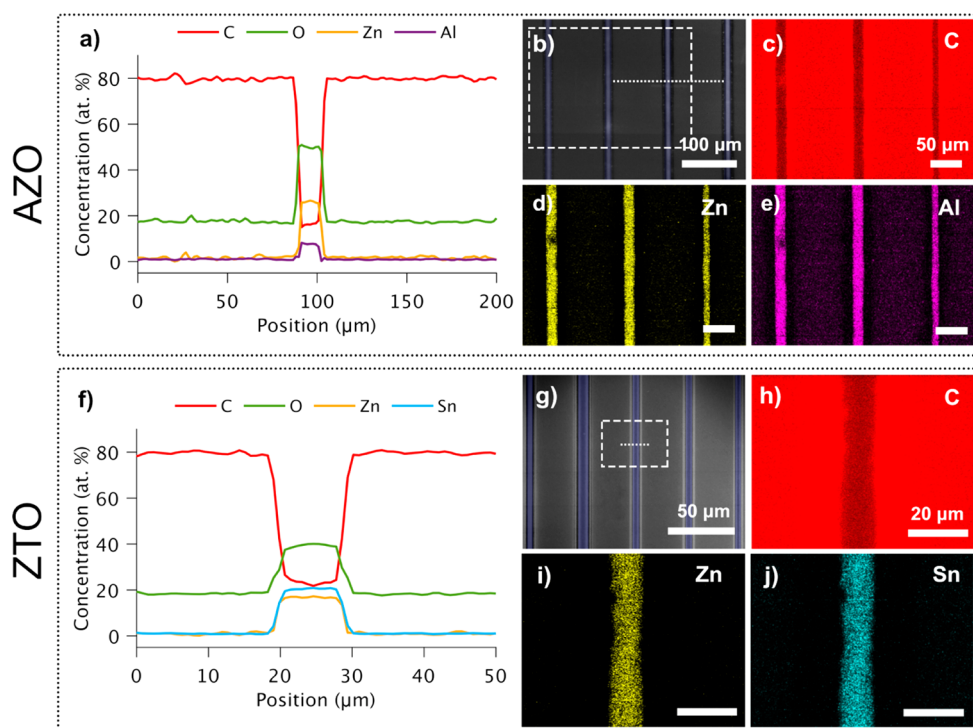
Figure 3. AES line scan of a subtractive printed PMMA pattern with 9 μm line width after (a) 10 supercycles of AZO (20 nm) and (f) 100 supercycles of ZTO (25 nm). (b and g) SEM images of the PMMA patterned sample with AES elemental map scans of key elements: (c–e) carbon, zinc, and aluminum, respectively for AZO sample and (h–j) carbon, zinc, and tin, respectively for ZTO sample.
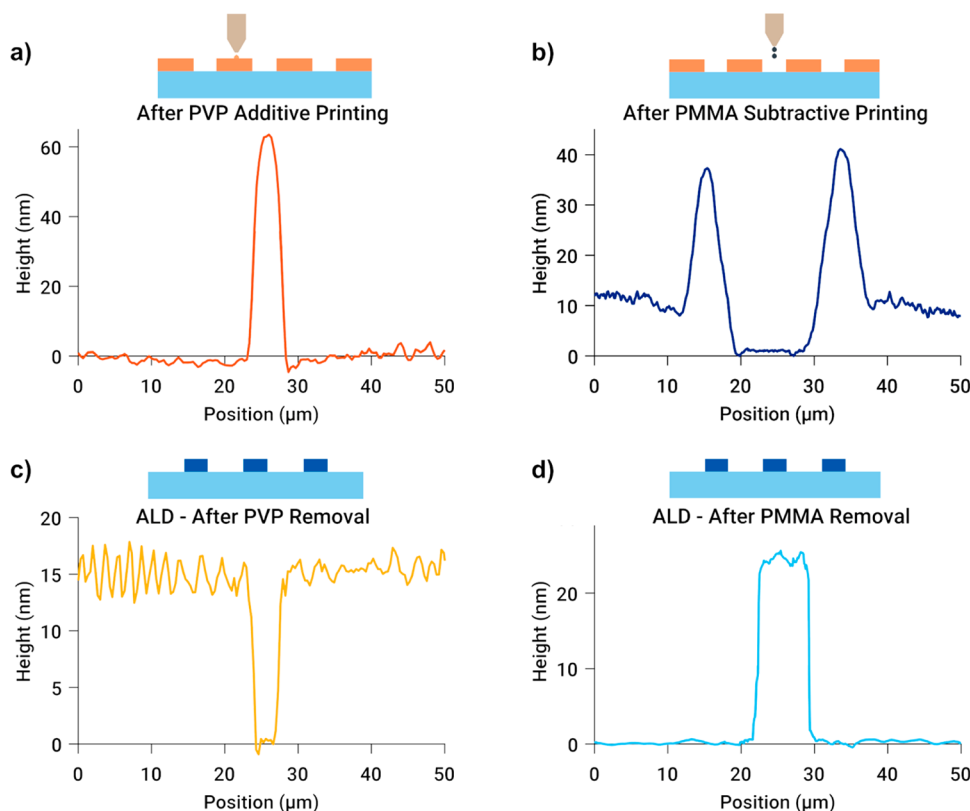

Figure 4. AFM scans of (a) additive e-jet printed PVP and (b) subtractive e-jet printed PMMA before ALD of AZO and ZTO, respectively; patterned ALD film (c) after AZO ALD and PVP removal, and (d) after ZTO ALD and PMMA removal. Note: the y-axis is shown at the nm-scale and x-axis is shown at the μm-scale.

Figure 2a shows AES line scans after 100 cycles of ZnO on an e-jet patterned square (shown in the SEM image in Figure

2b). Only C and O peaks are present on the PVP printed surface, demonstrating complete inhibition of ZnO. Within the

Scheme 2. Process Flow for Thin-Film-Transistor Fabrication with Subtractive and Additive e-Jet Printing[a]
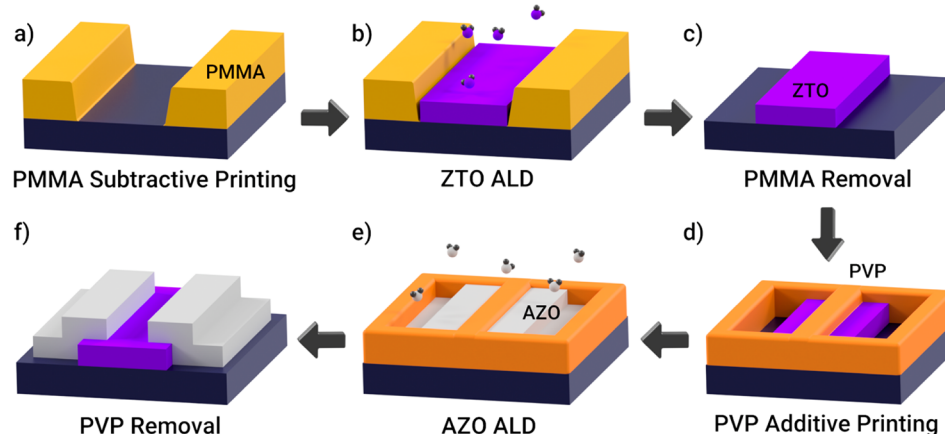
[a]Using subtractive e-jet printing (a), the semiconductor (ZTO) pattern was first defined (b). After PMMA removal and ZTO film anneal (c), PVP was additively-printed on top of the dielectric (SiO_2) and ZTO film to isolate and define the channel between the source and drain using AZO contacts (d). After selective depositon of AZO (e), PVP was removed to complete fabrication of the ZTO TFT (f).

unpatterned regions, the inverse is observed, where the C intensity drops significantly, and the Zn signal increases. Figure 2c and d shows elemental AES mapping of these patterns. The contrast between C and Zn is clearly shown in the AES map, demonstrating the selective growth of ternary oxide on the e-jet printed surface.

To illustrate the power of e-jet printing to pattern with sub-μm precision, PVP lines with a width of 312 ± 60 nm were printed and exposed to 10 supercycles of AZO (further details on the ALD process are provided in the Methods section). The resolution and the line width variation in e-jet printing depend on number of variables, including the electric field, ink material properties, and surface energy. Through control of these parameters, the ability to print sub-100 nm features is possible,[15] illustrating the potential to further improve the resolution and quality of printed features.

Zn and Al signals were only observed on the bare Si regions without PVP, whereas the inverse pattern was observed in the carbon map (Figure 2f−h). This line width resolution is 2 orders of magnitude higher than previous reports of electronic devices fabricated by AS-ALD and inkjet printing.[36,37]

To demonstrate the potential of subtractive printing to generate inverse patterns, a spin-coated PMMA surface was patterned by printing N-Methyl-2-pyrrolidone (NMP) as a solvent ink. This resulted in local dissolution and displacement of the polymer, exposing the underlying Si surface (Scheme 1). Compared with the AES line scan from additive printing, the opposite trend was observed for the subtractive-printed lines. Only C and O were detected on the unprinted PMMA surface, while AZO and ZTO were selectively deposited within the exposed regions (Figure 3a and 3f, respectively). Furthermore, in the elemental maps of patterned AZO, Zn and Al signals are only observed within the printed regions (Figure 3c−e). Similarly, only Zn and Sn are observed in the ZTO patterns. These results demonstrate selective patterning of ternary oxide films (Figure 3h−j).

One advantage of using subtractive printing for AS-ALD is that it enables localized ALD growth only within the printed region, without the need to print a wide passivation layer over the substrate. In this study, we demonstrated a line width of 9 μm using subtractive printing. Although subtractive e-jet printing has not been explored or optimized as widely as

additive e-jet printing, we anticipate that sub-μm resolution may be achievable in the future by carefully tuning jetting parameters and solvent−polymer chemical interactions.

To study the morphology of additive and subtractive e-jet printed structures, AFM scans were performed. No noticeable polymer deformation/reflow was detected when the PMMA was exposed to the ALD deposition temperature for 8 h (Figure S4). Using additive e-jet printing (Figure 4 a, c), planar AZO films grew on the entire silicon substrate surface except on the printed PVP line, which generated a trench that was 4 μm wide and 15 nm in height. For subtractive e-jet printing, a 9 μm wide trench of PMMA was patterned (Figure 4b) that was subsequently used to define the location of a 23 nm thick ZTO film. In Figure 4b, the subtractive-patterned PMMA profile exhibits side rims (~40 nm in height) adjacent to the trench. This is due to a coffee-ring effect during the solvent printing, which dissolved and displaced the original polymer (~12 nm in height) to the sides, while exposing the underlying silicon surface.[65−67]

After removal of the PMMA inhibition layer, a ZTO film with a rectangular cross section was left behind, as shown in Figure 4d. As shown for both additive and subtractive e-jet printing approaches, the ALD film grows only on the active surfaces of the substrate, rather than along the top or side surfaces of the polymer. This is a significant advantage over traditional lift-off processes using photolithography, which may result in remaining sidewalls on the patterned thin film. Therefore, the maximum height of the film in the z-direction before lateral spreading occurs is controlled by the thickness of the polymer. In contrast, area-selective ALD on a thin inhibitor layer may exhibit a "mushroom" geometry, which is attributed to the isotropic ALD growth, which is not inhibited in the lateral direction.[68] With e-jet patterned AS-ALD, the PVP thickness can be controlled by adjusting additive e-jet printing parameters, while the subtractive-printed PMMA thickness can easily be controlled during the spin coating.[14,15,69] This demonstrates the advantages of printing polymers for AS-ALD, as the inhibition of growth can be influenced in both the in-plane and out-plane directions.

The additive and subtractive e-jet/AS-ALD techniques can be combined to enable additive manufacturing of 3D architectures with deterministic control of geometry. To
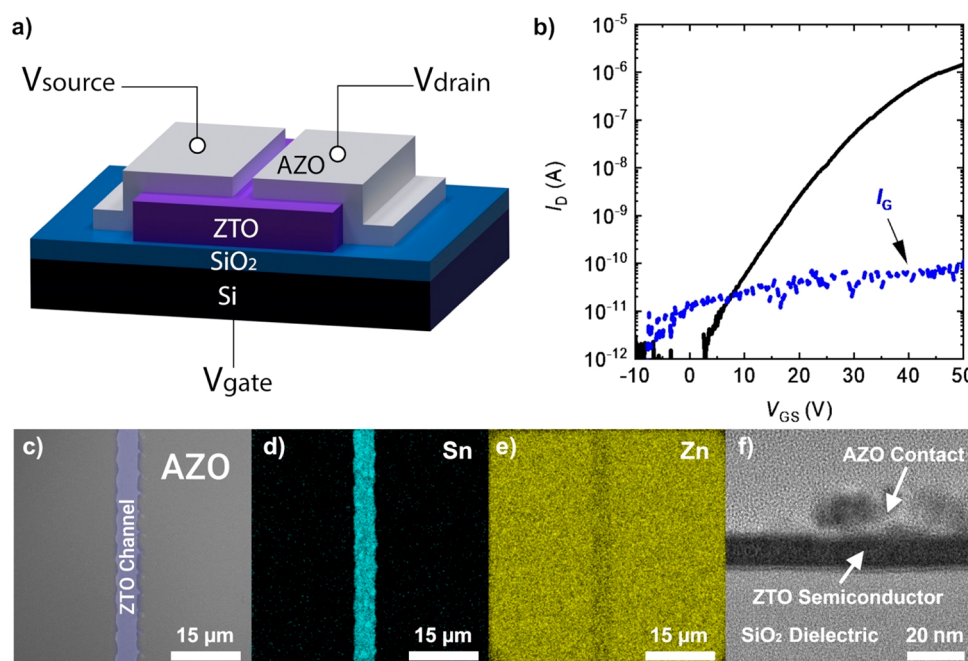
Figure 5. (a) Fabricated TFT structure. In this first generation of e-jet/AS-ALD printed TFTs, device isolation is achieved by ensuring that the AZO source and drain contacts are separate from other AZO regions on the sample, and are the only AZO features to contact the ZTO island. (b) Transfer curves of a 5-μm channel length device with V_{DS} = 1 V. (c) Top-down SEM image of a device with a 4-μm long channel with corresponding AES mapping of (d) Sn and (e) Zn. (f) Cross-sectional scanning transmission electron microscopy (STEM) image of a 4-μm channel device after selective AZO deposition using additive PVP printing.

demonstrate fabrication of 3D metal oxide structures by a combination of subtractive and additive printing techniques, we fabricated a bottom-gate top-contact ZTO TFT, as shown in Scheme 2. First, ZTO, the device active layer, was patterned on a Si substrate with a 100 nm SiO$_2$ thermal oxide using subtractive e-jet printing of a solvent on spin-coated PMMA. After removal of the ZTO inhibitor polymer, the ZTO film was annealed to improve its transport properties.[54] Finally, AZO, the source/drain contact electrode material, was patterned on top of the ZTO film using additive e-jet printing of PVP.

The final device structure is illustrated in Figure 5a and Figure S5. Electrical measurements of the first TFTs fabricated using e-jet and AS-ALD show that the devices are well-behaved (Figure 5b), with 0 V turn-on, on current >1 μA, and an on/off current ratio >10^5. The devices have a minimum channel length of approximately 5 μm, 1 order of magnitude smaller than what has been achieved previously for inkjet printed inhibitors for AS-ALD.[36,37] Thus, these devices demonstrate the ability to leverage the improved resolution of e-jet printing. In previous ALD ZTO film characterization, we have achieved electron mobility >22 cm^{2}V^{-1}s^{-1} in TFTs fabricated using traditional photolithography methods.[54] To successfully fabricate the e-jet and AS-ALD device in this initial demonstration, the ZTO ALD deposition temperature was reduced to 130 °C and thermal ALD was used, in order to maintain compatibility with the inhibitor polymers used here, at least partially contributing to a reduced mobility of approximately 0.12 cm^{2}V^{-1}s^{-1}. In the future, improved device performance can be achieved by optimizing the e-jet and AS-ALD processes to achieve higher ZTO mobility, and by tuning the AZO layer composition to reduce contact resistance.

AES mapping (Figure 5c−e) of a channel region shows that e-jet printing on top of the ZTO film (1) successfully blocks AZO growth to spatially confine the AZO film and (2) does

not affect the ZTO pattern, which is fabricated in a prior step. Sn is only observed in the TFT channel (due to the surface sensitivity of AES, the ZTO that lies under AZO is not visible). Inspecting the Zn AES signal, we note that the signal is stronger in the AZO region compared to the ZTO channel region. Since AZO is deposited with a 15:1 Zn to Al cycle ratio, AZO has higher Zn content than that of ZTO, which is why the Zn signal is slightly lower within the channel. This indicates that AZO has been selectively deposited in the source/drain ohmic contact regions. This patterned growth of AZO on top of ZTO is further shown by a cross-sectional STEM images in Figure 5f and Figure S5. These observations demonstrate that the combination of e-jet additive and subtractive printing can be used for 3D additive manufacturing of functional materials and devices.

CONCLUSION

In this work, we have introduced an additive manufacturing platform that combines AS-ALD with e-jet printing. After polymer patterning, ALD films with desired material composition can be selectively grown on passivated (additive-printed) or activated (subtractive-printed) surfaces. Using PVP and PMMA as the inhibition layers for AS-ALD, growth of different binary and ternary ALD films (ZnO, Al$_2$O$_3$, SnO$_2$, AZO, and ZTO) can be suppressed within their selectivity windows. This approach enables additive manufacturing with sub-μm resolution in the x−y plane and sub-nm resolution in the z-direction with tunable material composition and with fast printing speeds (~5 mm/s). To demonstrate manufacturing of functional devices using AS-ALD with e-jet printing, a bottom-gate, top-contact TFT was fabricated without photolithography. The TFTs showed well-defined transfer curves with an on/off current ratio of greater than 10^5.

As modern electronic devices increase in complexity, the combination of AS-ALD and e-jet printing represents a powerful fabrication platform for additive manufacturing. This process allows for customizable geometries and versatile material selection and is compatible with future deposition on nonplanar and/or flexible surfaces.[14] In the future, e-jet printing of polymer patterns could be combined with spatial ALD which could increase the throughput of the ALD step by a factor of >100.[37,41] Furthermore, in contrast to alternative printing processes, e-jet printing enables sub-μm patterning with orders of magnitude faster line speeds than most existing additive nanomanufacturing techniques.[1] This enables the possibility of manufacturing customizable devices for applications ranging from personalized healthcare to flexible electronics in a cost-effective manner. For example, for personalized health monitoring, there is a need to fabricate customized integrated systems due to specific physiological composition of each human. In the future, this platform can be applied to additive manufacturing of customizable integrated nanosystems, bridging materials and geometries to integrate multiple sub-systems and length-scales seamlessly.

METHODS

Atomic Layer Deposition. A custom-built, flow-type thermal ALD station was used to coat ZnO, Al$_2$O$_3$, and SnO$_2$. All depositions were performed at a temperature range of 100−170 °C. ZnO was deposited using diethylzinc (DEZ) and H$_2$O as precursors, with an argon carrier gas. Al$_2$O$_3$ was deposited using dimethylaluminum isopropoxide (DMAI). SnO$_2$ was deposited using tetrakis (diethylamino) tin(IV) (TDMASn). One cycle of binary oxide ALD consisted of precursor A pulse (0.05 s for DEZ and DMAI, 0.15 s for TDMASn), Ar purge (45 s), H$_2$O pulse (0.1 s), and Ar purge (45 s). One supercycle of ternary oxide ALD consisted of different ratios of binary oxide cycles. A 6:5 zinc/tin ratio for zinc tin oxide (ZTO) was used in Figures 5 and S2; a 1:1 zinc/tin ratio was used for Figures 1−4 and S1; a 10:1 zinc/aluminum ratio for aluminum-doped zinc oxide (AZO) was used for Figures 1−4 and S1; and a 15:1 zinc/ aluminum was used for Figures 5 and S2. In Figure 5b, the 5-μm channel device was deposited at 130 °C and the 4-μm channel device (shown in Figure 5c−f) was deposited with an ALD temperature of 170 °C. The argon carrier gas flow rate was set at 70 sccm. The growth rates of each binary and ternary oxide on a bare silicon substrate were measured using ellipsometry to be ZnO − 1.90 Å/ cycle, Al$_2$O$_3$ − 1.15 Å/cycle, SnO$_2$ − 0.88 Å/cycle, AZO − 2.01 Å/ supercycle, and ZTO − 2.52 Å/supercycle at a 130 °C deposition temperature.

Electrohydrodynamic Jet Patterning. An e-jet system with an integrated AFM measurements tool was a custom-made system by the Barton Research Group at the University of Michigan.[70] The nozzles for the e-jet process were made from pulled-glass from World Precision Instruments (WPI) and sputter-coated with 5 nm of gold to make them conductive. Moreover, they were coated in a hydrophobic solution (0.01% 1H, 1H, 2H, 2H-perfluorodecane-1-thio (PFDT) in dimethylformamide (DMF)) to avoid wetting of the nozzle body during printing. PVP was additively printed on a silicon substrate using 0.1 and 10 wt % PVP (0.1 wt % for sub-micron PVP printing and 10 wt % PVP for TFT channel printing) dissolved in dimethyl sulfoxide (DMSO) as the ink. We used nozzles with various sizes in this study: 1 μm nozzle size for sub-micron PVP, 2 μm nozzle size for PVP printing on the TFT channel, 5 μm nozzle for sub 10-μm subtractive patterns, and 10 μm nozzle for subtractive patterning of PMMA for ZTO in TFT fabrication.

To deposit a uniform layer of PMMA, a 950 MW 2% anisole− PMMA solution was spin-coated on a Si substrate. The substrate was coated at 4000 rpm for 45 s to form an approximately 65 nm thick film. After spin-coating, the sample was baked at 180 °C for 10 s to remove the anisole solvent. N-Methyl-2-pyrrolidone (NMP) from Sigma-Aldrich was used as the etching solvent for PMMA. Before subtractive e-jet printing, the PMMA coated silicon wafer was exposed to UV O$_3$ for 20 min to remove adventitious carbon and to improve solubility in NMP.[71] After subtractive e-jet printing of polymers, a 30 s O$_2$ plasma exposure (YES Plasma Stripper, 100 W, 66 sccm O$_2$, 47 sccm Ar, 50 °C) was used to remove any remaining residue of PMMA within the displaced region.

Film Characterization and Elemental Analysis. The ALD film thickness was measured by a J. A. Woollam M-2000 Ellipsometer with three angles of incidence (65°, 70°, and 75°) and was fit using a Cauchy model. AES line and map scans were recorded using a Phi 680 Auger Nanoprobe. A Kratos Axis Ultra XPS was used to perform XPS elemental analysis. XPS data were analyzed using the CasaXPS software package to determine the composition of the film. SEM images were taken using an FEI Helios 650 Nanolab SEM at 2 kV and 100 pA. AFM images were taken using a Veeco Dimension Icon Atomic Force Microscope with a ScanAsyst-Air AFM tip from Bruker Nano Inc. The data were analyzed using Nanoscope Analysis 2.0 software. Cross-sectional STEM samples were prepared via a lift-out process using an FEI Helios 650 Nanolab dualbeam FIB/SEM. STEM imaging was performed using a Thermo Fisher Talos F200X G2 S/ TEM at 200 kV. Prior to STEM-EDS, samples were tilted in TEM mode to align to the 100 zone axis of Si wafer substrate such that the interfaces were parallel to the beam direction. STEM-EDS was collected with 4 Super-X window-less detectors using Velox software (Thermo Fisher). A 2-pixel gaussian blur was applied to the raw EDS maps to create smoother composition profiles.

Thin Film Transistor Fabrication and Electrical Measurements. ZTO deposited for the channel layer was subjected to a 1 h 500°C post-deposition anneal before top AZO deposition, in ambient air with relative humidity less than 20%. Electrical measurements were taken in the dark at room temperature in ambient air using an HP4155A semiconductor parameter analyzer. The data were taken with continuous voltage sweeps and short integration. Forward $I−V$ sweeps were taken by sweeping V_{GS} from negative to positive.

ASSOCIATED CONTENT

ⓢ Supporting Information

The Supporting Information is available free of charge at https://pubs.acs.org/doi/10.1021/acsnano.0c07297.

> XPS analysis of PMMA/PVP coated samples, AFM analysis of the PMMA after exposing it to ALD deposition temperature, and the cross-sectional STEM image of the polymers and the TFT device (PDF)

AUTHOR INFORMATION

Corresponding Authors

Neil P. Dasgupta − *Department of Mechanical Engineering and Department of Materials Science & Engineering, University of Michigan, Ann Arbor, Michigan 48109, United States;* ⓞ orcid.org/0000-0002-5180-4063; Email: ndasgupt@umich.edu

Kira Barton − *Department of Mechanical Engineering, University of Michigan, Ann Arbor, Michigan 48109, United States;* Email: bartonkl@umich.edu

Rebecca L. Peterson − *Department of Electrical Engineering and Computer Science and Department of Materials Science & Engineering, University of Michigan, Ann Arbor, Michigan 48109, United States;* ⓞ orcid.org/0000-0001-9405-6539; Email: blpeters@umich.edu

Authors

Tae H. Cho − *Department of Mechanical Engineering, University of Michigan, Ann Arbor, Michigan 48109, United States*

Nazanin Farjam − *Department of Mechanical Engineering, University of Michigan, Ann Arbor, Michigan 48109, United States*

Christopher R. Allemang − *Department of Electrical Engineering and Computer Science, University of Michigan, Ann Arbor, Michigan 48109, United States*

Christopher P. Pannier − *Department of Mechanical Engineering, University of Michigan, Ann Arbor, Michigan 48109, United States*

Eric Kazyak − *Department of Mechanical Engineering, University of Michigan, Ann Arbor, Michigan 48109, United States*

Carli Huber − *Department of Materials Science & Engineering, University of Michigan, Ann Arbor, Michigan 48109, United States*

Mattison Rose − *Department of Mechanical Engineering, University of Michigan, Ann Arbor, Michigan 48109, United States*

Orlando Trejo − *Department of Mechanical Engineering, University of Michigan, Ann Arbor, Michigan 48109, United States*

Complete contact information is available at:
https://pubs.acs.org/10.1021/acsnano.0c07297

Notes

The authors declare no competing financial interest.

REFERENCES

(1) Engstrom, D. S.; Porter, B.; Pacios, M.; Bhaskaran, H. Additive Nanomanufacturing - A Review. *J. Mater. Res.* **2014**, *29*, 1792−1816.

(2) Zhakeyev, A.; Wang, P.; Zhang, L.; Shu, W.; Wang, H.; Xuan, J. Additive Manufacturing: Unlocking the Evolution of Energy Materials. *Adv. Sci.* **2017**, *4*, 1700187.

(3) Hiramoto, T. Five Nanometre CMOS Technology. *Nat. Electron.* **2019**, *2*, 557−558.

(4) Piner, R. D.; Zhu, J.; Xu, F.; Hong, S.; Mirkin, C. A. Dip-Pen" Nanolithography. *Science* **1999**, *283*, 661−664.

(5) Eigler, D. M.; Schweizer, E. K. Positioning Single Atoms with Scanning Tunnelling Microscope. *Nature* **1990**, *344*, 524−526.

(6) Zhang, Y. L.; Chen, Q. D.; Xia, H.; Sun, H. B. Designable 3D Nanofabrication by Femtosecond Laser Direct Writing. *Nano Today* **2010**, *5*, 435−448.

(7) Deubel, M.; Von Freymann, G.; Wegener, M.; Pereira, S.; Busch, K.; Soukoulis, C. M. Direct Laser Writing of Three-Dimensional Photonic-Crystal Templates for Telecommunications. *Nat. Mater.* **2004**, *3*, 444−447.

(8) Derby, B. Inkjet Printing of Functional and Structural Materials: Fluid Property Requirements, Feature Stability, and Resolution. *Annu. Rev. Mater. Res.* **2010**, *40*, 395−414.

(9) Gao, M.; Li, L.; Song, Y. Inkjet Printing Wearable Electronic Devices. *J. Mater. Chem. C* **2017**, *5*, 2971−2993.

(10) Noh, Y. Y.; Zhao, N.; Caironi, M.; Sirringhaus, H. Downscaling of Self-Aligned, All-Printed Polymer Thin-Film Transistors. *Nat. Nanotechnol.* **2007**, *2*, 784−789.

(11) Sirringhaus, H.; Kawase, T.; Friend, R. H.; Shimoda, T.; Inbasekaran, M.; Wu, W.; Woo, E. P. High-Resolution Inkjet Printing of All-Polymer Transistor Circuits. *Science* **2000**, *290*, 2123−2126.

(12) Li, Y.; Lan, L.; Xiao, P.; Sun, S.; Lin, Z.; Song, W.; Song, E.; Gao, P.; Wu, W.; Peng, J. Coffee-Ring Defined Short Channels for Inkjet-Printed Metal Oxide Thin-Film Transistors. *ACS Appl. Mater. Interfaces* **2016**, *8*, 19643−19648.

(13) Shao, F.; Wan, Q. Recent Progress on Jet Printing of Oxide-Based Thin Film Transistors. *J. Phys. D: Appl. Phys.* **2019**, *52*, 143002.

(14) Park, J. U.; Hardy, M.; Kang, S. J.; Barton, K.; Adair, K.; Mukhopadhyay, D. K.; Lee, C. Y.; Strano, M. S.; Alleyne, A. G.; Georgiadis, J. G.; Ferreira, P. M.; Rogers, J. A. High-Resolution Electrohydrodynamic Jet Printing. *Nat. Mater.* **2007**, *6*, 782−789.

(15) Onses, M. S.; Sutanto, E.; Ferreira, P. M.; Alleyne, A. G.; Rogers, J. A. Mechanisms, Capabilities, and Applications of High-Resolution Electrohydrodynamic Jet Printing. *Small* **2015**, *11*, 4237−4266.

(16) Lee, S.; Kim, J.; Choi, J.; Park, H.; Ha, J.; Kim, Y.; Rogers, J. A.; Paik, U. Patterned Oxide Semiconductor by Electrohydrodynamic Jet Printing for Transparent Thin Film Transistors. *Appl. Phys. Lett.* **2012**, *100*, 102108.

(17) Jeong, S.; Lee, J. Y.; Lee, S. S.; Seo, Y. H.; Kim, S. Y.; Park, J. U.; Ryu, B. H.; Yang, W.; Moon, J.; Choi, Y. Metal Salt-Derived In-Ga-Zn-O Semiconductors Incorporating Formamide as a Novel Co-Solvent for Producing Solution-Processed, Electrohydrodynamic-Jet Printed, High Performance Oxide Transistors. *J. Mater. Chem. C* **2013**, *1*, 4236−4243.

(18) Lee, Y. G.; Choi, W. S. Electrohydrodynamic Jet-Printed Zinc-Tin Oxide TFTs and Their Bias Stability. *ACS Appl. Mater. Interfaces* **2014**, *6*, 11167−11172.

(19) Dasgupta, N. P.; Lee, H.-B.-R.; Bent, S. F.; Weiss, P. S. Recent Advances in Atomic Layer Deposition. *Chem. Mater.* **2016**, *28*, 1943−1947.

(20) George, S. M. Atomic Layer Deposition: An Overview. *Chem. Rev.* **2010**, *110*, 111−131.

(21) Sheng, J.; Lee, J.-H.; Choi, W.-H.; Hong, T.; Kim, M.; Park, J.-S. Review Article: Atomic Layer Deposition for Oxide Semiconductor Thin Film Transistors: Advances in Research and Development. *J. Vac. Sci. Technol., A* **2018**, *36*, 060801.

(22) Mackus, A. J. M.; Merkx, M. J. M.; Kessels, W. M. M. From the Bottom-Up : Toward Area-Selective Atomic Layer Deposition with High Selectivity. *Chem. Mater.* **2019**, *31*, 2−12.

(23) Lee, H. B. R.; Bent, S. F. A Selective Toolbox for Nanofabrication. *Chem. Mater.* **2020**, *32*, 3323−3324.

(24) Parsons, G. N.; Clark, R. D. Area-Selective Deposition: Fundamentals, Applications, and Future Outlook. *Chem. Mater.* **2020**, *32*, 4920−4953.

(25) Lee, W.; Dasgupta, N. P.; Trejo, O.; Lee, J.; Hwang, J.; Usui, T.; Prinz, F. B. *Langmuir* **2010**, *26*, 6845−6852.

(26) Mackus, A. J. M.; Dielissen, S. A. F.; Mulders, J. J. L.; Kessels, W. M. M. Nanopatterning by Direct-Write Atomic Layer Deposition. *Nanoscale* **2012**, *4*, 4477−4480.

(27) Chen, R.; Kim, H.; McIntyre, P. C.; Porter, D. W.; Bent, S. F. Achieving Area-Selective Atomic Layer Deposition on Patterned Substrates by Selective Surface Modification. *Appl. Phys. Lett.* **2005**, *86*, 191910.

(28) Ellinger, C. R.; Nelson, S. F. Selective Area Spatial Atomic Layer Deposition of ZnO, Al_2O_3, and Aluminum-Doped ZnO Using Poly (vinyl Pyrrolidone). *Chem. Mater.* **2014**, *26*, 1514−1522.

(29) Fang, M.; Ho, J. C. Area-Selective Atomic Layer Deposition: Conformal Coating, Subnanometer Thickness Control, and Smart Positioning. *ACS Nano* **2015**, *9*, 8651−8654.

(30) Sinha, A.; Hess, D. W.; Henderson, C. L. Area Selective Atomic Layer Deposition of Titanium Dioxide: Effect of Precursor Chemistry. *J. Vac. Sci. Technol. B Microelectron. Nanom. Struct.* **2006**, *24*, 2523−2532.

(31) Cheng, N.; Banis, M. N.; Liu, J.; Riese, A.; Li, X.; Li, R.; Ye, S.; Knights, S.; Sun, X. Extremely Stable Platinum Nanoparticles Encapsulated in a Zirconia Nanocage by Area-Selective Atomic

Layer Deposition for the Oxygen Reduction Reaction. *Adv. Mater.* **2015**, *27*, 277−281.

(32) Mackus, A. J. M.; Bol, A. A.; Kessels, W. M. M. The Use of Atomic Layer Deposition in Advanced Nanopatterning. *Nanoscale* **2014**, *6*, 10941−10960.

(33) Jiang, X.; Bent, S. F. Area-Selective ALD with Soft Lithographic Methods: Using Self-Assembled Monolayers to Direct Film Deposition. *J. Phys. Chem. C* **2009**, *113*, 17613−17625.

(34) Mameli, A.; Karasulu, B.; Verheijen, M. A.; Barcones, B.; Macco, B.; Mackus, A. J. M.; Kessels, W. M. M. E.; Roozeboom, F. Area-Selective Atomic Layer Deposition of ZnO by Area Activation Using Electron Beam-Induced Deposition. *Chem. Mater.* **2019**, *31*, 1250−1257.

(35) Mameli, A.; Kuang, Y.; Aghaee, M.; Ande, C. K.; Karasulu, B.; Creatore, M.; Mackus, A. J. M.; Kessels, W. M. M.; Roozeboom, F. Area-Selective Atomic Layer Deposition of In$_2$O$_3$:H Using a μ-Plasma Printer for Local Area Activation. *Chem. Mater.* **2017**, *29*, 921−925.

(36) Levy, D. H.; Ellinger, C. R.; Nelson, S. F. Metal-Oxide Thin-Film Transistors Patterned by Printing. *Appl. Phys. Lett.* **2013**, *103*, 043505.

(37) Nelson, S. F.; Ellinger, C. R.; Levy, D. H. Improving Yield and Performance in ZnO Thin-Film Transistors Made Using Selective Area Deposition. *ACS Appl. Mater. Interfaces* **2015**, *7*, 2754−2759.

(38) Bobb-Semple, D.; Nardi, K. L.; Draeger, N.; Hausmann, D. M.; Bent, S. F. Area-Selective Atomic Layer Deposition Assisted by Self-Assembled Monolayers: A Comparison of Cu, Co, W, and Ru. *Chem. Mater.* **2019**, *31*, 1635−1645.

(39) Chen, R.; Kim, H.; McIntyre, P. C.; Bent, S. F. Investigation of Self-Assembled Monolayer Resists for Hafnium Dioxide Atomic Layer Deposition. *Chem. Mater.* **2005**, *17*, 536−544.

(40) Hashemi, F. S. M.; Prasittichai, C.; Bent, S. F. A New Resist for Area Selective Atomic and Molecular Layer Deposition on Metal-Dielectric Patterns. *J. Phys. Chem. C* **2014**, *118*, 10957−10962.

(41) Poodt, P.; Cameron, D. C.; Dickey, E.; George, S. M.; Kuznetsov, V.; Parsons, G. N.; Roozeboom, F.; Sundaram, G.; Vermeer, A. Spatial Atomic Layer Deposition: A Route Towards Further Industrialization of Atomic Layer Deposition. *J. Vac. Sci. Technol., A* **2012**, *30*, 010802.

(42) Richey, N. E.; De Paula, C.; Bent, S. F. Understanding Chemical and Physical Mechanisms in Atomic Layer Deposition. *J. Chem. Phys.* **2020**, *152*, 040902.

(43) Xu, Y.; Musgrave, C. B. A DFT Study of the Al$_2$O$_3$ Atomic Layer Deposition on SAMs: Effect of SAM Termination. *Chem. Mater.* **2004**, *16*, 646−653.

(44) Ande, C. K.; Knoops, H. C. M.; De Peuter, K.; Van Drunen, M.; Elliott, S. D.; Kessels, W. M. M. Role of Surface Termination in Atomic Layer Deposition of Silicon Nitride. *J. Phys. Chem. Lett.* **2015**, *6*, 3610−3614.

(45) Parsons, G. N. Functional Model for Analysis of ALD Nucleation and Quantification of Area-Selective Deposition. *J. Vac. Sci. Technol., A* **2019**, *37*, 020911.

(46) Färm, E.; Kemell, M.; Ritala, M.; Leskelä, M. Selective-Area Atomic Layer Deposition Using Poly (Methyl Methacrylate) Films as Mask Layers. *J. Phys. Chem. C* **2008**, *112*, 15791−15795.

(47) Färm, E.; Kemell, M.; Santala, E.; Ritala, M.; Leskelä, M. Selective-Area Atomic Layer Deposition Using Poly (vinyl Pyrrolidone) as a Passivation Layer. *J. Electrochem. Soc.* **2010**, *157*, K10−K14.

(48) Vervuurt, R. H. J.; Sharma, A.; Jiao, Y.; Kessels, W. M. M.; Bol, A. A. Area-Selective Atomic Layer Deposition of Platinum Using Photosensitive Polyimide. *Nanotechnology* **2016**, *27*, 405302.

(49) Pattison, T. G.; Hess, A. E.; Arellano, N.; Lanzillo, N.; Nguyen, S.; Bui, H.; Rettner, C.; Truong, H.; Friz, A.; Topuria, T.; Fong, A.; Hughes, B.; Tek, A. T.; DeSilva, A.; Miller, R. D.; Qiao, G. G.; Wojtecki, R. J. Surface Initiated Polymer Thin Films for the Area Selective Deposition and Etching of Metal Oxides. *ACS Nano* **2020**, *14*, 4276−4288.

(50) Chen, Y.; Ginga, N. J.; LePage, W. S.; Kazyak, E.; Gayle, A. J.; Wang, J.; Rodríguez, R. E.; Thouless, M. D.; Dasgupta, N. P. Enhanced Interfacial Toughness of Thermoplastic-Epoxy Interfaces Using ALD Surface Treatments. *ACS Appl. Mater. Interfaces* **2019**, *11*, 43573−43580.

(51) Leng, C. Z.; Losego, M. D. Vapor Phase Infiltration (VPI) for Transforming Polymers into Organic-Inorganic Hybrid Materials: A Critical Review of Current Progress and Future Challenges. *Mater. Horiz.* **2017**, *4*, 747−771.

(52) Choi, I. M.; Kim, M. J.; On, N.; Song, A.; Chung, K. B.; Jeong, H.; Park, J. K.; Jeong, J. K. Achieving High Mobility and Excellent Stability in Amorphous In-Ga-Zn-Sn-O Thin-Film Transistors. *IEEE Trans. Electron Devices* **2020**, *67*, 1014−1020.

(53) Baek, I. H.; Pyeon, J. J.; Han, S. H.; Lee, G. Y.; Choi, B. J.; Han, J. H.; Chung, T. M.; Hwang, C. S.; Kim, S. K. High-Performance Thin-Film Transistors of Quaternary Indium-Zinc-Tin Oxide Films Grown by Atomic Layer Deposition. *ACS Appl. Mater. Interfaces* **2019**, *11*, 14892−14901.

(54) Allemang, C. R.; Cho, T. H.; Trejo, O.; Ravan, S.; Rodríguez, R. E.; Dasgupta, N. P.; Peterson, R. L. High-Performance Zinc Tin Oxide TFTs with Active Layers Deposited by Atomic Layer Deposition. *Adv. Electron. Mater.* **2020**, *6*, 2000195.

(55) Kazyak, E.; Chen, K. H.; Wood, K. N.; Davis, A. L.; Thompson, T.; Bielinski, A. R.; Sanchez, A. J.; Wang, X.; Wang, C.; Sakamoto, J.; Dasgupta, N. D. Atomic Layer Deposition of the Solid Electrolyte Garnet Li$_7$La$_3$Zr$_2$O$_{12}$. *Chem. Mater.* **2017**, *29*, 3785−3792.

(56) Bielinski, A. R.; Lee, S.; Brancho, J. J.; Esarey, S. L.; Gayle, A. J.; Kazyak, E.; Sun, K.; Bartlett, B. M.; Dasgupta, N. P. Atomic Layer Deposition of Bismuth Vanadate Core-Shell Nanowire Photoanodes. *Chem. Mater.* **2019**, *31*, 3221−3227.

(57) Mackus, A. J. M.; Schneider, J. R.; Macisaac, C.; Baker, J. G.; Bent, S. F. Synthesis of Doped, Ternary, and Quaternary Materials by Atomic Layer Deposition: A Review. *Chem. Mater.* **2019**, *31*, 1142−1183.

(58) Cho, M. H.; Seol, H.; Song, A.; Choi, S.; Song, Y.; Yun, P. S.; Chung, K. B.; Bae, J. U.; Park, K. S.; Jeong, J. K. Comparative Study on Performance of IGZO Transistors With Sputtered and Atomic Layer Deposited Channel Layer. *IEEE Trans. Electron Devices* **2019**, *66*, 1783−1788.

(59) Sheng, J.; Hong, T. H.; Lee, H. M.; Kim, K. R.; Sasase, M.; Kim, J.; Hosono, H.; Park, J. S. Amorphous IGZO TFT with High Mobility of 70 cm^2/(V s) *via* Vertical Dimension Control Using PEALD. *ACS Appl. Mater. Interfaces* **2019**, *11*, 40300−40309.

(60) Heo, J.; Kim, S. B.; Gordon, R. G. Atomic Layer Deposited Zinc Tin Oxide Channel for Amorphous Oxide Thin Film Transistors. *Appl. Phys. Lett.* **2012**, *101*, 113507.

(61) Warner, E. J.; Johnson, F.; Campbell, S. A.; Gladfelter, W. L. Atomic Layer Deposition of Tin Oxide and Zinc Tin Oxide Using Tetraethyltin and Ozone. *J. Vac. Sci. Technol., A* **2015**, *33*, 021517.

(62) Hu, W.; Peterson, R. L. Molybenum as a Contact Material in Zinc Tin Oxide Thin Film Transistors. *Appl. Phys. Lett.* **2014**, *104*, 192105.

(63) Dasgupta, N. P.; Neubert, S.; Lee, W.; Trejo, O.; Lee, J. R.; Prinz, F. B. Atomic Layer Deposition of Al-Doped ZnO Films: Effect of Grain Orientation on Conductivity. *Chem. Mater.* **2010**, *22*, 4769−4775.

(64) Banerjee, P.; Lee, W. J.; Bae, K. R.; Lee, S. B.; Rubloff, G. W. Structural, Electrical, and Optical Properties of Atomic Layer Deposition Al-Doped ZnO Films. *J. Appl. Phys.* **2010**, *108*, 043504.

(65) Deegan, R. D.; Bakajin, O.; Dupont, T. F.; Huber, G.; Nagel, S. R.; Witten, T. A. Capillary Flow as the Cause of Ring Stains from Dried Liquid Drops. *Nature* **1997**, *389*, 827−829.

(66) Majumder, M.; Rendall, C. S.; Eukel, J. A.; Wang, J. Y. L.; Behabtu, N.; Pint, C. L.; Liu, T. Y.; Orbaek, A. W.; Mirri, F.; Nam, J.; Barron, A. R.; Hauge, R. H.; Schmidt, H. K.; Pasquali, M. Overcoming the "Coffee-Stain" Effect by Compositional Marangoni-Flow-Assisted Drop-Drying. *J. Phys. Chem. B* **2012**, *116*, 6536−6542.

(67) Farjam, N.; Cho, T. H.; Dasgupta, N. P.; Barton, K. Subtractive Patterning: High-Resolution Electrohydrodynmaic Jet Printing with Solvents. *Appl. Phys. Lett.* **2020**, *117*, 133702.

(68) Lee, H.; Bent, S. F. Nanopatterning by Area-Selective Atomic Layer Deposition. In *Atomic Layer Deposition of Nanostructured Materials*; Pinna, N., Knez, M., Eds.; Wiley-VCH Verlag GmbH & Co. KGaA: Weinheim, Germany, 2012; pp 193−225.

(69) Semaltianos, N. G. Spin-Coated PMMA Films. *Microelectron. J.* **2007**, *38*, 754−761.

(70) Pannier, C. P.; Ojeda, L.; Wang, Z.; Hoelzle, D.; Barton, K. An Electrohydrodynamic Jet Printer with Integrated Metrology. *Mechatronics* **2018**, *56*, 268−276.

(71) Park, E. S. *Application of Inkjet-Printing Technology to Micro-Electro-Mechanical Systems*. Doctoral dissertation, University of California at Berkley, Berkley, CA, 2013.